

# A comparison of sea level projections based on the observed and reconstructed sea level data around the Korean Peninsula

Kwang-Yul Kim<sup>1</sup> · Yeonjoo Kim<sup>2</sup>

Received: 7 January 2016 / Accepted: 8 January 2017 / Published online: 27 March 2017  
© Springer Science+Business Media Dordrecht 2017

**Abstract** In an attempt to estimate accurate local sea level change, “sea level trend” modes are identified and separated from natural variability via cyclostationary empirical orthogonal function (CSEOF) analysis applied to both the tide gauge data (1965–2013) and the reconstruction data (1950–2010) around the Korean Peninsula. For the tide gauge data, ensemble empirical mode decomposition (EEMD) method is also used to estimate sea level trend to understand an uncertainty from different analysis tools. The three trend models—linear, quadratic, and exponential—are fitted to the amplitude time series of the trend mode so that future projection of sea level can be made. Based on a quadratic model, the rate of local sea level rise (SLR) is expected to be  $4.63 \pm 1.1 \text{ mm year}^{-1}$  during 2010–2060. The estimates of “local” sea level trend vary up to ~30%. It should be noted that, although the three trend models estimate similar sea level trends during the observational period, the projected sea level trend and subsequent SLR differ significantly from one model to another and between the tide gauge data and the reconstruction data; this results in a substantial uncertainty in the future SLR around the Korean Peninsula.

## 1 Introduction

Much attention has been given to the issue of global mean sea level (GMSL) rise, including the rate of acceleration, over the last two centuries (Boon 2012). The latest Intergovernmental Panel on Climate Change Report (Church et al. 2013) (hereafter referred to IPCC 2013 Report) estimated the GMSL rise during the past century to have been approximately  $1.7 \text{ mm year}^{-1}$ . Recent estimates of sea level (SL) acceleration based on GMSL dating back to the 1700s and

---

**Electronic supplementary material** The online version of this article (doi:10.1007/s10584-017-1901-8) contains supplementary material, which is available to authorized users.

---

✉ Yeonjoo Kim  
yeonjoo.kim@yonsei.ac.kr

<sup>1</sup> School of Earth and Environmental Sciences, Seoul National University, Seoul, Republic of Korea

<sup>2</sup> Department of Civil and Environmental Engineering, Yonsei University, Seoul, Republic of Korea

1800s range from  $0.009 \pm 0.003 \text{ mm year}^{-2}$  (Church and White 2011) to  $0.013 \pm 0.006 \text{ mm year}^{-2}$  (Church and White 2006). There is an obvious indication that the rate of sea level rise (SLR) is accelerating.

Estimate of the rate of SLR around the Korean Peninsula varies significantly from one study to another, mainly because of the lack of long and reliable gauge measurement; there are only a few gauge measurements of SL dating back to the early 1960s. Cho (2002) estimated an average SLR rate to be  $2.310 \pm 2.220 \text{ mm year}^{-1}$  after correcting vertical land movement due to postglacial rebound; tide gauge measurements in 1960–1999 at 23 stations were used for this estimate. Youn et al. (2004) estimated an average SLR rate of  $2.8 \text{ mm year}^{-1}$  during 1981–2000 based on nine tide gauge stations selected by anomaly coherency analysis. Using the TOPEX/Poseidon SL data as well as tide gauge data, Kang et al. (2005) investigated the patterns of SLR in the East Sea. The estimated mean trend using tide gauge data is  $2.9 \pm 0.7 \text{ mm year}^{-1}$  for 26 years (1977–2002) and  $6.6 \pm 3.3 \text{ mm year}^{-1}$  for 9 years (1993–2001). Further, Kim and Cho (2015) used the ensemble empirical mode decomposition (EEMD) technique to estimate the SLR rate and its acceleration at five tide gauge stations around the Korean Peninsula. They showed that the estimated SLR varied significantly from one station to another from  $0.35 \text{ mm year}^{-1}$  at Mukho (1965–2011) to  $5.03 \text{ mm year}^{-1}$  at Jeju (1964–2011).

While the Archiving, Validation and Interpretation of Satellite Oceanographic (AVISO) dataset has a global coverage, its record length is relatively short. Alternately, historical measurements of SL from tide gauges extend back to the beginning of the nineteenth century (Holgate et al. 2013). On the other hand, tide gauges are generally sparse, particularly before 1950. By combining the dense spatial coverage of satellite altimetry and the long record length of the tide gauges, it is possible to reconstruct global SL to examine longer time scale climate signals and assess their contributions to SL both regionally and globally (e.g., Chambers et al. 2002; Church et al. 2004; Hamlington et al. 2011a). These reconstructions interpolate in situ tide gauge measurements back in time using basis functions derived from satellite altimetry data or model data. For example, Hamlington et al. (2011b) reconstructed SL for 1950–2010 using the cyclostationary empirical orthogonal function (CSEOF) technique. The reconstruction datasets serve as useful means of estimating past and current SL trends and important baselines for evaluating model-based SL projections.

According to the SL reconstruction data and coupled climate model simulations, the SLR rate has been accelerating and this acceleration will likely continue in the twenty-first century. A range of projections of GMSL is given in the IPCC 2013 Report for each climate change scenario. Regional and local SL trends, however, differ significantly from the global SL trend, and SL projection on a local or regional level is not easy to access. Further, there is no strong confidence in the models' ability to simulate regional SLR in an accurate manner. On the other hand, there are typically not a sufficient number of tide gauges around the regions of interest for an accurate estimation of SL trends. Further, tide gauge record varies in length from one station to another and is contaminated by non-uniform correction for postglacial isostatic adjustment. This situation is exacerbated by much higher level of regional/local natural variability than that of global SL (Hamlington et al. 2014). As a result, estimation of SL trend on a regional/local level is much more difficult and is prone to serious errors.

The AVISO satellite products are known to be somewhat inaccurate along the coasts, and this inaccuracy may be reflected in the reconstruction data as well. However, there has been a lack of serious attempts to delineate actual differences between tide gauge measurements and reconstruction data on a regional level. In a recent study, Hamlington et al. (2015) showed that their reconstruction is reasonably accurate around the coast of the USA in comparison with the tide

gauge measurements. If SL reconstruction dataset is shown to be reasonably accurate along the coasts, it can be a useful tool for addressing local/regional SL change both present and future.

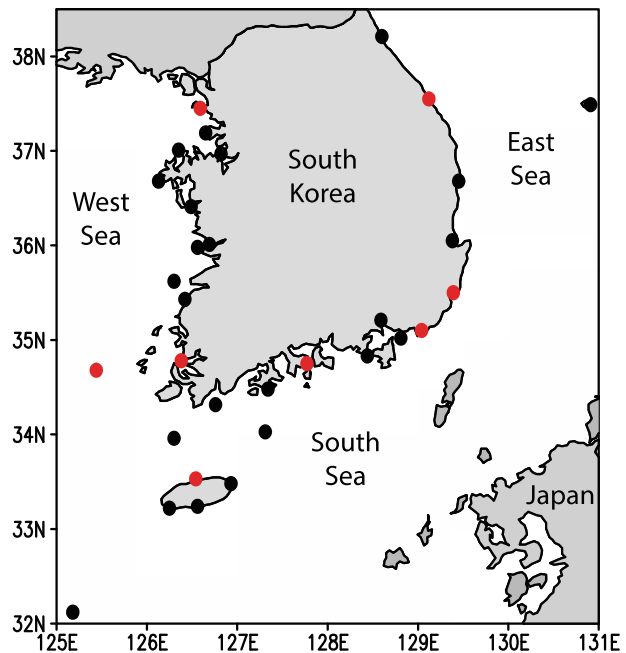
Thus, in this study, the rate of SL trend around the Korean Peninsula is estimated by using both tide gauge measurements and SL reconstruction and the difference between the two types of data is addressed in terms of SL trends on a local or regional level. As a primary analysis tool, the CSEOF technique (Kim et al. 1996; Kim and North 1997) is employed to isolate the trend mode; this allows us to estimate rigorously the rate and acceleration of SLR due to global warming without any serious contamination by natural variability. For tide gauge measurements, we estimate the SL trends with the EEMD technique (Wu and Huang 2009) in addition to the CSEOF technique and compare the two estimates for understanding the uncertainty of the estimates arising from the difference in analysis techniques. At last, SLR around the Korean Peninsula is projected until 2060 to address the uncertainty of SL estimates arising from data quality and the method of projection.

## 2 Data and methods of analysis

### 2.1 Data

The data used for this study is the SL measurements archived at Korea Hydrographic and Oceanographic Administration. This study uses tide gauge data only at 8 of the 32 stations, for which SL data are available from 1965 without serious missing data (Fig. 1). Table S1 of the Electronic supplementary material (ESM) shows the exact locations and lengths of observations at the 8 stations.

**Fig. 1** The location of the 32 tide gauge measurements around the Korean Peninsula archived at the Korea Hydrographic and Oceanographic Administration. The sea level measurements at these 8 tide gauges (*red dots*), where the measurements are available from 1965 or earlier, are used



Also used is the  $0.5^\circ \times 0.5^\circ$  global SL reconstruction from 1950 to 2010 by Hamlington et al. (2011b) archived at NASA/JPL Physical Oceanography Distributed Active Archive Center. Tide gauge observations of SL prior to the AVISO measurements are used for generating the global SL dataset. This dataset appears to be reasonably accurate in comparison with the existing SL reconstruction dataset (Strassburg et al. 2014) and with the tide gauges around the USA (Hamlington et al. 2015).

## 2.2 CSEOF analysis

Both the observation and reconstruction data are subject to CSEOF analysis (Kim et al. 1996; Kim and North 1997). In CSEOF analysis, whose details are explained in S1 of ESM, space-time data is decomposed into the  $n$  CSEOF mode number of cyclostationary loading vectors (CSLVs) and the principal component (PC) time series. Unlike EOF analysis, CSLVs are time dependent and periodic. The primary purpose of CSEOF analysis is to separate the mode representing SL trend from other naturally occurring SL variability. The latter contaminates the SL trend and the rate of acceleration, particularly on a regional and local level.

## 2.3 Autoregressive modeling

Once CSEOF analysis is completed, SL data will be extended into the future based on the trend in each PC time series (details in S2 of ESM). The trend is identified by fitting three different models to each PC time series. The three trend models for the  $n$ th PC time series include linear, quadratic, and exponential models. Then, synthetic PC time series can be constructed to have statistical properties that are (nearly) identical with that of the detrended PC time series.

Given an autoregressive (AR) model for each PC time series, we can generate synthetic PC time series by using different realizations. Then, synthetic datasets including trends can be constructed and by adding the trend in each PC time series, the resulting synthetic dataset is a statistical prediction of SL based on the assumed trend.

## 2.4 EEMD method

In addition to the CSEOF technique, this study also uses the EEMD method (Wu and Huang 2009) to estimate SL trend from the observations at the tide gauge stations around the Korean Peninsula. The EEMD method is used to obtain an independent estimate of SLR and ensure that the estimate in the present study is not sensitive to the analysis technique employed. The details of EEMD are explained in S3 of ESM. Recently, several studies (e.g., Breaker and Ruzmaikin 2011; Ezer et al. 2013; Breaker and Ruzmaikin 2013; Kim and Cho 2015) utilized the EEMD or empirical model decomposition (EMD) methods to analyze SL change in different regions, including the USA and Korea.

# 3 Results and discussion

## 3.1 CSEOF analysis of regional sea surface level

A primary motivation of CSEOF analysis is to separate the SL trend mode from other naturally occurring modes. CSEOF analysis was conducted on the regional SL reconstruction data with

the nested period of 12 months. The domain of analysis is [117°–140° E × 32°–45° N] representing the marginal seas around the Korean Peninsula. Data to the south and east of Japan are excluded, since the strong SL variability associated with the Kuroshio obscures variability in the marginal seas (see Fig. S1).

The 12-month averaged loading vectors for the first four CSEOF modes and the corresponding PC time series are shown in Fig. 2a, b, respectively. These four modes together explain ~85% of the total SL variability in the reconstruction data. As can be

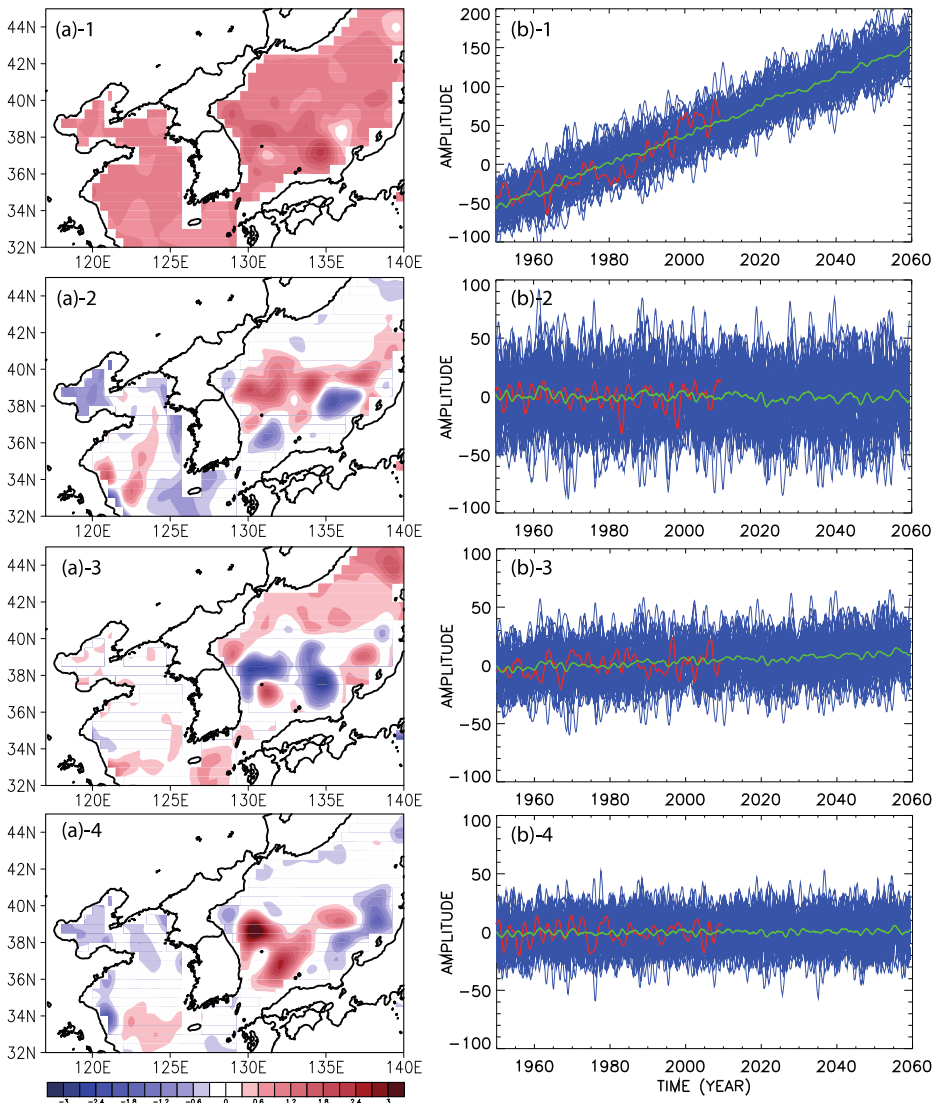


**Fig. 2** a Spatial patterns of 12-month averages from the first four CSEOF modes derived of the 1950–2010 sea level reconstruction data. b The PC time series from the first four CSEOF modes of 1950–2010 sea level reconstruction data (red curves), and 100 different synthetic PC time series from 1950 to 2060 (blue curves), and the averaged synthetic PC time series (green curves)

seen, the first CSEOF mode, explaining ~73% of the total variability, depicts increasing SL over the marginal seas. Judging from the corresponding PC time series, this mode represents the effect of ocean warming as a result of climate change (see e.g., Figure 8 of Na et al. 2012; Fig. 6 of Seo et al. 2014) and mass loading on SL. The second CSEOF mode is correlated with the NINO3 and Pacific Decadal Oscillation (PDO) indices at 0.464 and 0.391, respectively. While this mode is consistent with the finding of Gordon and Giulivi (2004), who noted a connection between the SL change in the East/Japan Sea and the PDO variability in the North Pacific, the second mode is more highly correlated with the NINO3 index. The other modes in Fig. 2 seem to be associated primarily with the ocean fronts at ~38°–40° N, the intricate circulation and bathymetry in the East/Japan Sea (see e.g., Na et al. 2010, 2012; Fig. 15 of Seo et al. 2014). The detailed physical interpretation for regional SL variability is difficult and is considered beyond the scope of this study.

### 3.2 Synthetic time series of CSEOF modes

Based on the CSEOF modes, we constructed synthetic SL. We used the first 20 CSEOF modes, which explain 98.8% of the total variability in the 1950–2010 SL reconstruction dataset aside from the seasonal cycle. As in Table S2, which shows the parameters of the trend models identified from each PC time series, the modes beyond the first 20 explain less than 0.2% of the total variability and do not help explaining the variability of SL. Note that the rate of change of the local trend (first) mode is more than 10 times the rates of the other modes (Fig. 2). Therefore, the assumption of a specific type of trend does not affect other than the global trend mode in any serious manner.

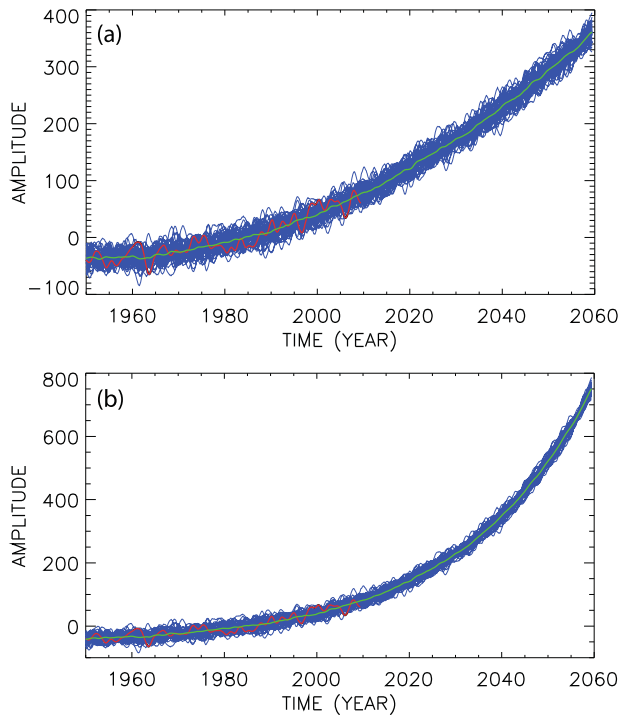
Then, an AR model was fitted to each PC time series after removing the trend. Table S3 shows the order and the ratio of error variance to the variance of each PC time series. It shows that error variance is typically less than 1% of the variance of each PC time series; thus, the resulting AR model should be a close representation of each PC time series.

Using the identified AR model, total of 100 synthetic PC time series were generated, as in Equation (S7), based on 100 different realizations of regression error time series. Then, the removed trend was added back to the synthetic time series. Figure 2 shows the synthetic time series for each of the first four PC time series based on the linear trend model. The original PC time series is within the spread of the 100 synthetic time series, which allows us to determine a more robust trend model and estimate uncertainty in the future projection of SL arising from the randomness of the timing and magnitude of natural variability.

In particular, the first CSEOF mode represents the effect of local warming on SLR. As can be seen in Fig. 2b (1), the linear trend predicts that the amplitude of the first PC time series increases at the rate of  $15.7 \times 10^{-2}$  per month, or equivalently, 1.887 per year. In conjunction with the loading vector in Fig. 2a (1), this rate is translated into an average of 1.82 mm year<sup>-1</sup> in the marginal seas. In the linear trend model, there is no acceleration in the SLR.

Figure 3 shows the projections of the first PC time series based on the quadratic and exponential trend models. These two models account for the acceleration of SL trend. As warming progresses, ice-sheet albedo feedback and increased mass loading cause the

**Fig. 3** The projected first PC time series (global trend mode) based on the quadratic trend model (*upper panel*) and the exponential trend model (*lower panel*). The *red curve* is the original PC time series, the *blue curves* represent the 50 synthetic PC time series, and the *green curve* is the average of the 50 synthetic time series



acceleration of SLR (e.g., Hu et al. 2010). According to these two models, the slope of the trend is given respectively by

$$\frac{dY_1(t)}{dt} = 2a_q^{(1)}t + b_q^{(1)} = 69.04 \times 10^{-3}t + 1.64 \times 10^{-1}, \tag{1}$$

$$\frac{dY_1(t)}{dt} = a_e^{(1)}b_e^{(1)}\exp\left(b_e^{(1)}t\right) = 16.69 \times 35.45 \times 10^{-3}\exp\left(35.45 \times 10^{-3}t\right), \tag{2}$$

where  $t$  is time in years since 1950. The mean SLR rate during the observational period (1950–2010) is 2.24 and 2.06 mm year<sup>-1</sup> for the quadratic and exponential trend models, respectively. The mean trends for the quadratic and exponential models are slightly larger than that of the linear trend model over the observational period (1950–2010). As of 2010, the SLR rate is 4.31 and 4.96 mm year<sup>-1</sup> for the quadratic and exponential models, respectively. During the prediction period (2010–2060), the SLR rate is 6.03 and 13.68 mm year<sup>-1</sup> for the two models, respectively. Thus, the quadratic model expects ~3 times and the exponential model ~7 times faster SLR than the linear model for the prediction period.

The mean acceleration rate is  $6.90 \times 10^{-2}$  mm year<sup>-2</sup> for the quadratic trend model; thus, the SLR rate increases by  $6.90 \times 10^{-2}$  mm year<sup>-1</sup> every year. For the exponential trend model, the mean acceleration rate is  $7.29 \times 10^{-2}$  mm year<sup>-2</sup> during the observational period and  $48.5 \times 10^{-2}$  mm year<sup>-2</sup> for the prediction period. Thus, the SL trend increases, on average, by  $4.85 \times 10^{-1}$  mm year<sup>-1</sup> every year during the prediction period of 2010–2060 according to the exponential trend model. The exponential model predicts ~7 times higher mean



acceleration rate than the quadratic model in the prediction period. Note that the SL estimates based on the three different trend models are significantly different. Unfortunately, the three models fit the observed SLR equally well and, henceforth, the difference among the three estimates represents uncertainty in the future SL estimates.

Figures 2b and 3 show that the PC time series from the reconstruction dataset fits reasonably in the range of synthetic PC time series in Equation (S9). All three trend models employed in this study result in a good representation of the effect of global warming in the data. Unfortunately, however, this also means that a reasonable model cannot be identified by the regression error alone, and that a robust rate of acceleration cannot be determined from the data. Because of the ambiguous acceleration rate, therefore, the range of uncertainty in the future estimates of SL bounds to be fairly wide. As in Table 1, local SLR with respect to the 1950–1960 average during 2051–2060 is 185, 350, and 658 mm for the linear, quadratic, and exponential trend models, respectively. The quadratic model predicts 1.9 times higher change in GMSL than the linear model, and the exponential model results in ~2 times higher estimate than the quadratic model by 2060. Uncertainty due to natural variability in the estimate of SL change is fairly low: less than 10% in the linear model and less than 3% for the other two models.

Regional pattern of SL change is also examined. Figure S1 shows the 10-year (2050–2059) averaged SL change in the marginal seas around the Korean Peninsula. As expected, spatial inhomogeneity of SL change within the marginal seas of the Korean Peninsula is not negligible at all. SLR in the marginal seas appears to be 36–52% higher than that of the global oceans. This seems to be consistent with inhomogeneous warming in the global oceans and greater warming in the marginal seas around the Korean Peninsula than the average warming of the global oceans (Yeo and Kim 2014).

### 3.3 A comparison with the tide gauge observations

CSEOF analysis was conducted on the tide gauge observations around the Korean Peninsula. Only 8 out of 32 gauges were used, since those 8 gauges have reasonably long observations without serious missing values (Fig. 1 and Table S1). The tide gauge data from 1965 to 2013 are analyzed after minor missing observations are filled via interpolations. Also selected from the SL reconstruction data were the grid points closest to these 8 tide gauges. Then, CSEOF analysis was conducted on both datasets.

The first CSEOF mode of the tide gauge data turns out to be the seasonal cycle (Fig. 4a). The loading vector of the seasonal cycle shows that SL is maximum in August and minimum in February. The corresponding PC time series shows that the amplitude of the seasonal cycle

**Table 1** Averaged sea level change around the Korean Peninsula with respect to the 1950–1960 average according to the linear, quadratic, and exponential trend models

Decade	Linear	Quadratic	Exponential
2001–2010	93.7 (13.3)	96.3 (7.9)	99.2 (7.7)
2011–2020	111.4 (12.4)	134.7 (7.4)	149.1 (7.2)
2021–2030	130.5 (11.4)	180.5 (6.7)	221.1 (6.5)
2031–2040	147.8 (13.3)	231.7 (8.0)	322.5 (7.9)
2041–2050	167.6 (14.4)	291.0 (8.6)	468.5 (8.3)
2051–2060	184.5 (13.9)	350.3 (8.3)	657.6 (8.1)

The values in parenthesis denote one standard deviation among the 100 ensemble members (unit: mm)



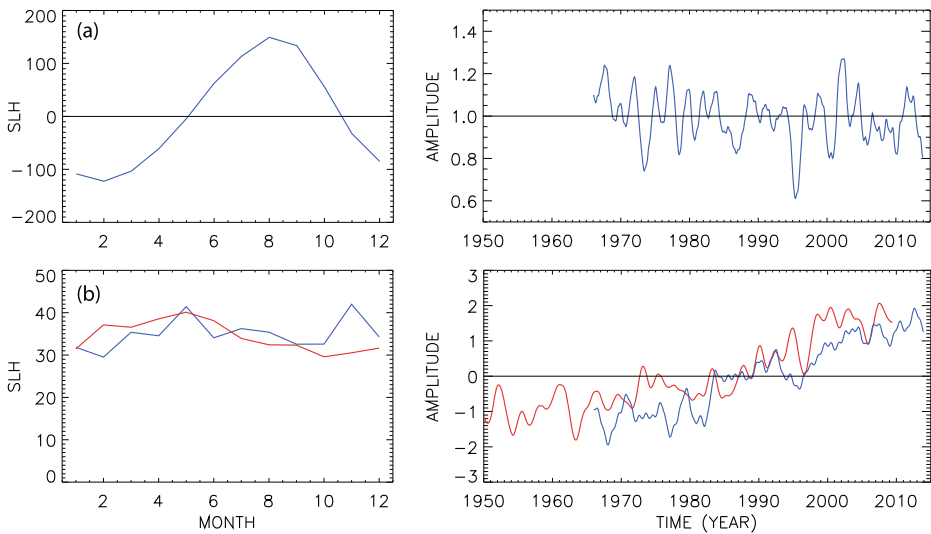


**Fig. 4** The (left) loading vector and (right) PC time series of **a** the seasonal cycle based on the tide gauge data and **b** the trend mode based on the tide gauge data (blue) and the reconstruction data (red)

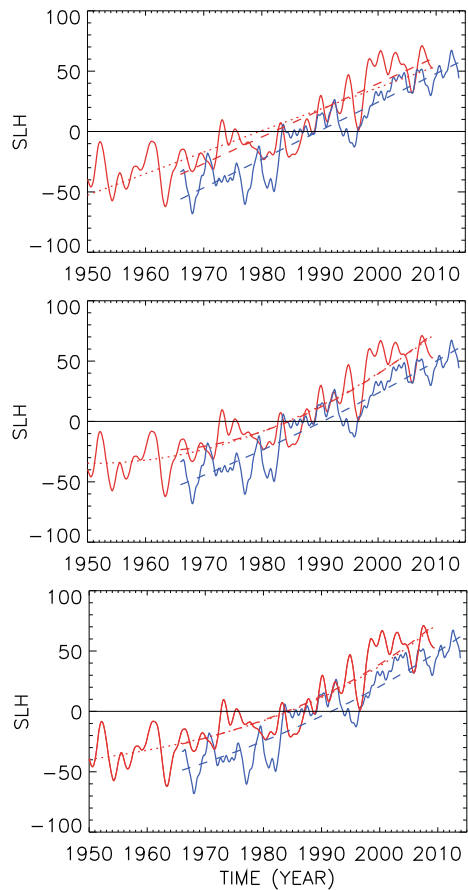
fluctuates by about  $\pm 10\%$ . There is no corresponding mode in the reconstruction data, since the seasonal cycle is not included in the dataset (Hamlington et al. 2011b).

The second CSEOF mode represents the “local” trend mode (Fig. 4b). The loading vector averaged over the eight spatial points does not exhibit strong seasonality both for the tide gauge data and the reconstruction data. The PC time series shows a conspicuous trend. Correlation between the two PC time series in Fig. 4b is 0.89; high correlation between the two time series derives primarily from the trend in the time series. After detrending, correlation decreases to 0.29 indicating that the fluctuations on top of the trend are not quite similar between the two time series. Nonetheless, the trends and their slopes seem reasonably similar between the two time series.

Based on the two PC time series and the loading vector of the local trend mode, station-averaged SLR around the Korean Peninsula has been generated as in Fig. 5. Then, SL trends have been identified as discussed above in Table S4. The average rate of SLR during 1965–2010 is 2.364, 2.337, and 2.320  $\text{mm year}^{-1}$  for the observational data and is 2.225, 2.248, and 2.321  $\text{mm year}^{-1}$  for the reconstruction data. Thus, the SLR rate based on the two different datasets is very similar. Also, the deviation among different trend models is fairly small ( $< 0.14 \text{ mm year}^{-1}$ ) in the observational period.

The SLR rate in 2010, however, differs significantly between different trend models: 2.364, 2.759, and 3.009  $\text{mm year}^{-1}$  for the observational data and 2.225, 4.032, and 4.229  $\text{mm year}^{-1}$  for the reconstruction data. The projected mean SLR rate during 2010–2060 is 2.364, 3.228, and 4.137  $\text{mm year}^{-1}$  for the tide gauge data and is 2.213, 6.014, and 9.813  $\text{mm year}^{-1}$  for the reconstruction data. The total increment by 2060 from that in 1965 is 225, 267, and 455 mm for the observational data and is 211, 402, and 632 mm for the reconstruction data. For the linear trend model, there is little difference between the two datasets. SLR for the quadratic and exponential trend models based on the reconstruction data, however, is much higher than that based on the tide gauge data; specifically, estimates based on the reconstruction data are 135 and 177 mm higher than those based on the tide gauge data. It appears that the curvature of SL

**Fig. 5** Sea level change due to global warming derived from the tide gauge data (*blue*) and that derived from the reconstruction data (*red*) and (*upper panel*) a linear fit, (*middle panel*) a quadratic fit, and (*bottom panel*) an exponential fit based on the tide gauge data (*blue*), entire reconstruction data (*red dotted*), and reconstruction data from 1968 (*red dashed*)



change differs rather significantly between the two datasets. Thus, not only the rate but also the amount of SLR differs appreciably depending on the trend model and the data employed during the projection period.

According to the tide gauge data, the SLR rates at 8 stations are 0.46,  $-0.23$ , 0.49, 2.06, 0.35, 0.65, 0.93, and 3.30 times the mean rate addressed above. Thus, the Jeju station expects about 2 times and the Mokpo station more than 3 times the mean SL change. SL is expected to decrease at the Daehuksando station. The reconstruction data, however, does not show such remarkable spatial inhomogeneity. The SLR at the 8 closest grid points are 0.89, 0.95, 1.03, 1.01, 1.05, 1.08, 1.03, and 0.97 times the mean rate (Fig. 5). This is an expected result, since correlations between the tide gauge data and the reconstruction data are generally low ( $<0.5$ ) except at 3 stations (Table S1), and also correlations among the 8 stations are generally low. Thus, the trend estimates at individual stations can be seriously different between the two datasets; deviations at individual stations are much more significant than the deviation in station-averaged estimates. The situation does not change appreciably by using the grid points closest to the 32 stations; regional SL change is in the range of 0.8 and 1.3 of the mean SL change around the Korean Peninsula. Thus, much higher SLR is expected at Jeju and Mokpo stations based on the tide gauge data than that derived from the reconstruction data.

### 3.4 A comparison with the EEMD method

EEMD method was used to find the trend signal from the tide gauge data. The SL time series at the 8 stations were averaged, and the seasonal cycle was removed by using the composite analysis. Then, the gravest signal was extracted by using the EEMD method. Figure 6 shows the SL change identified by the EEMD method together with the linear and quadratic fits to the local trend mode (red dashed curves in Fig. 5). As can be seen, the EEMD curve is similar to the linear and quadratic fits, but the curvature is slightly larger than the quadratic fit to the trend mode of the tide gauge data. The quadratic fit to the EEMD curve is given by

$$Y_{obs}^{(emd)}(t) = -45.9 + 1.179t + 2.463 \times 10^{-2}t^2. \quad (3)$$

According to this quadratic polynomial, the mean SLR during 1965–2010 is  $2.287 \text{ mm year}^{-1}$ , which is slightly lower than the estimate based on the quadratic model of the local trend mode derived from the tide gauges. In 2010, the trend of the EEMD curve is  $3.396 \text{ mm year}^{-1}$ . During 2010–2060, SL trend is estimated to be  $4.627 \text{ mm year}^{-1}$ . Thus, the SL trends based on the EEMD method are larger than those based on the quadratic fit of the local trend mode. As a result, SL is expected to rise 288 mm from the mean SL in 1965, which is 21 mm higher than the quadratic fit of the local trend mode based on the tide gauge data and is 114 mm lower than that based on the reconstruction data. Overall, the trends estimated by the EEMD method agree better with those based on the quadratic fit to the local trend mode; the EEMD estimates are between the quadratic fits to the observational data and the reconstruction data (Table 2).

## 4 Summary and concluding remarks

CSEOF analysis was conducted on the reconstruction data to address the rate of SLR around the Korean Peninsula. CSEOF analysis identifies the local trend mode and the amplitude (PC) time series exhibits a distinct upward trend. Then, the trend of the PC time series of the local trend mode was determined by using three different assumptions of linear, quadratic, and exponential trends, representing essentially three different scenarios ranging from no acceleration (linear) to full feedback (exponential) in the acceleration of SL trend. Based on the trend of the local trend mode, the SLR was projected until 2060. By generating 100 different projections, uncertainty in the estimates of trend due to natural variability was also dealt with.

**Fig. 6** Sea level change due to local trend mode (*black solid*) with a linear fit (*black dashed*), quadratic fit (*red*), and EEMD curve (*blue*). The *dotted curve* represents the averaged sea level anomaly for the 8 tide gauge stations

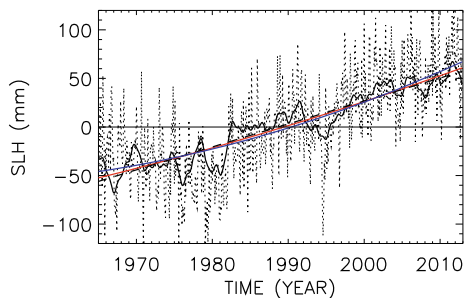


**Table 2** Comparison of the trends ( $\text{mm year}^{-1}$ ) and sea level rise (mm) between the local trend mode and the EEMD results. The local trend mode is computed from both the tide gauge data (OBS) and the reconstruction data (REC), and the three trend models are fitted to the local trend mode. The EEMD analysis is applied only to the tide gauge data

		Linear	Quad	Expo	EEMD
1965–2010 trend	OBS	2.364	2.337	2.320	2.287
	REC	2.225	2.248	2.321	
2010 trend	OBS	2.364	2.759	3.009	3.396
	REC	2.225	4.032	4.229	
2010–2060 trend	OBS	2.364	3.228	4.137	4.627
	REC	2.213	6.014	9.813	
2060 sea level	OBS	225	267	455	288
	REC	211	402	632	

CSEOF analysis was also conducted on the SL observations from 1965 at eight tide gauges around the Korean Peninsula. The PC time series of the trend mode of local SL variability shows a conspicuous trend. The PC time series derived from the tide gauges compares favorably with that derived from the reconstruction data.

While all three trend models are equally well fitted to the domain-averaged SL and results in similar trends during the record period, the quadratic model of the GMSL matches best with the projection in the IPCC 2013 Report (Figs. S2 and S3). Based on the quadratic trend model, mean SL trend around the Korean Peninsula in the observational period 1965–2010 is estimated to be 2.34, 2.25, 2.29, and 2.24  $\text{mm year}^{-1}$  for the local trend mode of the tide gauge data, the trend mode of the reconstruction data at 8 stations, the EEMD mode, and the regional trend mode. These estimates differ by a maximum of 2.9%. Thus, a robust estimate of current trend can be obtained from both the tide gauge data and the reconstruction data. These estimates are comparable to the estimate of  $2.310 \pm 2.22 \text{ mm year}^{-1}$  by Cho (2002) based on 23 gauge measurements in 1960–1999 and  $2.8 \text{ mm year}^{-1}$  by Youn et al. (2004) using 9 gauge measurements in 1981–2000. On the other hand, these estimates are significantly different from the estimate of  $6.6 \pm 3.3 \text{ mm year}^{-1}$  by Kang et al. (2005).

The SLR rate in 2010 in the Korean marginal seas is estimated to be 2.76, 4.03, 3.40, and 4.31  $\text{mm year}^{-1}$ . The mean SLR rate is  $3.63 \pm 0.7 \text{ mm year}^{-1}$  for 2010. The SLR rate does not differ by more than 20% of the mean value. During 2010–2060, the SLR rate increases to 3.23, 6.01, 4.63, and 6.03  $\text{mm year}^{-1}$  with the mean rate of  $4.98 \pm 1.3 \text{ mm year}^{-1}$ . The SL trend estimates vary by up to ~30%. The rate of acceleration is 1.88, 7.93, 4.93, and  $6.90 \times 10^{-2} \text{ mm year}^{-2}$  during 2010–2060 yielding a mean rate of  $5.41 \pm 2.7 \times 10^{-2} \text{ mm year}^{-2}$ . The acceleration rate varies by maximum of ~65% among the different estimates. SL is expected to rise by 267, 402, 288, and 350 mm by 2060 giving rise to a mean value of  $327 \pm 61 \text{ mm}$ . SLR in 2060 varies by ~23% of its mean value. Specifically, the trend estimated from the reconstruction data is higher than that estimated from the tide gauge data. The EEMD method applied to the station-averaged tide gauge time series results in consistently higher estimates than those based on the local trend mode of the tide gauge data but are consistently lower than those based on the local trend mode of the reconstruction data.

While the current trend of SLR around the Korean Peninsula is reliably estimated from different datasets by employing different techniques, future projections exhibit a relatively wide uncertainty. A primary reason is the difference in the acceleration rate of SLR between different datasets and different estimation techniques. The acceleration rate of SLR is

susceptible to error in the presence of relatively strong natural variability (Hamlington et al. 2016). In order to eliminate the effect of natural variability, trend was estimated from the trend mode, which was separated from other naturally occurring modes via CSEOF analysis. It is obvious from Fig. 6 that natural variability obfuscates the trend significantly and a conscientious effort should be made to eliminate natural variability as in this study. Despite such an effort, uncertainty remains to be relatively large.

Our estimates define a wider range of uncertainty than the IPCC 2013 Report (details in S4 of ESM; Figs. S2 and S3). While it is difficult to justify that future SLR around the Korean Peninsula will have the same trend with the observed, the range of GMSL rise based on the regression models looks reasonable considering the uncertainties of the process-based models and the forcing scenarios used in the IPCC 2013 Report. Further, estimates of regional SLR are an important factor for the adaptation/mitigation policy making, since they are not readily available in the IPCC 2013 Report except at a limited number of locations. Of course, the results of the present study should be understood with the inherent limitation of the statistical approach in mind.

Note that there are significant differences in the SL trend among the 8 tide gauge stations. Both CSEOF and EEMD analyses applied to the tide gauge data yield widely varying trends for individual tide gauges. On the other hand, there is relatively mild spatial variation of trend in the SL reconstruction data. It is not clear at all whether this spatial inhomogeneity is real or a sampling artifact. Hamlington et al. (2015) suggested that the reconstruction data is fairly reasonable in comparison with the measurements at tide gauges along the coast of the USA. This data quality issue should be addressed in order to describe SL change in marginal seas with any definitiveness. Furthermore, CSEOF analysis shows that the second mode is correlated with the NINO3 and PDO indices, which is not fully explained in previous studies. In a future study, detailed physical interpretation of the second CSEOF mode for regional SL variability should be fully addressed.

**Acknowledgments** This work was funded by the Korea Meteorological Administration Research and Development Program under Grant KMIPA 2015-6180 to Yeonjoo Kim as well as the SNU-Yonsei Research Cooperation Program through Seoul National University to Kwang-Yul Kim. The datasets used in this study can be acquired by writing an email to the corresponding author.

## References

- Breaker LC, Ruzmaikin A (2011) The 154-year record of sea level at San Francisco: Extracting the long-term trend, recent changes, and other tidbits. *Clim Dyn* 36(3):545–559. doi:10.1007/s00382-010-0865-4
- Breaker LC, Ruzmaikin A (2013) Estimating rates of acceleration based on the 157-year record of sea level from San Francisco, California, U.S.A. *J Coast Res* 29(1):43–51. doi:10.2112/JCOASTRES-2-0048.1
- Boon JD (2012) Evidence of sea level acceleration at U.S. and Canadian tide stations, Atlantic Coast, North America. *J Coast Res* 28(6):1437–1445
- Chambers DP, Mehlhaff CA, Urban TJ, Fujii D, Nerem RS (2002) Low-frequency variations in global mean sea level: 1950–2000. *J Geophys Res* 107(C4). doi:10.1029/2001JC001089
- Cho K (2002) Sea-level trend at the Korean coast. *J Environ Sci* 11(11):1141–1147
- Church JA, White NJ (2006) A 20th century acceleration in global sea-level rise. *Geophys Res Lett* 33:L01602. doi:10.1029/2005GL024826
- Church JA, White NJ (2011) Sea-level rise from the late 19th to the early 21st century. *Surv Geophys* 32:585–602
- Church J, White N, Coleman R, Lambeck K, Mitrovica J (2004) Estimates of the regional distribution of sea level rise over the 1950–2000 period. *J Clim* 17:2609–2625

- Church JA, Clark PU, Cazenave A, Gregory JM, Jevrejeva S, Levermann A, Merrifield MA, Milne GA, Nerem RS, Nunn PD, Payne AJ, Pfeffer WT, Stammer D, Unnikrishnan AS (2013) Sea level change. In: Climate change 2013: the physical science basis. Contribution of working group I to the fifth assessment report of the intergovernmental panel on climate change. Cambridge, United Kingdom and New York, NY, USA: Cambridge University Press.
- Ezer TL, Atkinson P, Corlett WB, Blanco JL (2013) Gulf stream's induced sea level rise and variability along the U.S. mid-Atlantic coast. *J Geophys Res Oceans* 118:685–697. doi:[10.1002/jgrc.20091](https://doi.org/10.1002/jgrc.20091)
- Gordon AL, Giulivi CF (2004) Pacific decadal oscillation and sea level in the Japan/East Sea. *Deep Sea Res* 51: 653–663
- Hamlington BD, Leben RR, Nerem RS, Kim K-Y (2011a) The effect of signal-to-noise ratio on the study of sea level trends. *J Clim* 24:1396–1408
- Hamlington BD, Leben RR, Nerem RS, Han W, Kim K-Y (2011b) Reconstructing sea level using cyclostationary empirical orthogonal functions. *J Geophys Res Oceans* 116:C12015. doi:[10.1029/2011JC007529](https://doi.org/10.1029/2011JC007529)
- Hamlington BD, Strassburg MW, Leben RR, Han W, Nerem RS, Kim K-Y (2014) Uncovering the anthropogenic sea level rise signal in the Pacific Ocean. *Nat Clim Chang*. doi:[10.1038/nclimate2307](https://doi.org/10.1038/nclimate2307)
- Hamlington BD, Leben RR, Kim K-Y, Nerem RS, Atkinson LP, Thompson PR (2015) The effect of the El Niño-southern oscillation on coastal and regional sea level in the United States. *J Geophys Res Oceans*. doi:[10.1002/2014JC010602](https://doi.org/10.1002/2014JC010602)
- Hamlington BD, Cheon SH, Thompson PR, Merrifield MA, Nerem RS, Leben RR, Kim K-Y (2016) An ongoing shift in Pacific Ocean sea level. *J Geophys Res Oceans* 121:5084–5097. doi:[10.1002/2016JC011815](https://doi.org/10.1002/2016JC011815)
- Holgate SJ, Matthews A, Woodworth PL, Rickards LJ, Tamisiea ME, Bradshaw E, Foden PR, Gordon KM, Jevrejeva S, Pugh J (2013) New data systems and products at the permanent service for mean sea level. *J Coast Res* 29(3):493–504
- Hu A, Meehl GA, Otto-Bliessner BL, Waelbroeck C, Han W, Loutre M-F, Lambeck K, Mitrovica JX, Rosenbloom N (2010) Influence of Bering Strait flow and North Atlantic circulation on glacial sea-level changes. *Nat Geosci*. doi:[10.1038/NGEO729](https://doi.org/10.1038/NGEO729)
- Kang SK, Cherniawsky JY, Foreman MGG, Min HS, Kim C-H, Kang H-W (2005) Patterns of recent sea level rise in the East/Japan Sea from satellite altimetry and in situ data. *J Geophys Res* 110:C07002. doi:[10.1029/2004JC002565](https://doi.org/10.1029/2004JC002565)
- Kim Y, Cho K (2015) Sea level rise around Korea: analysis of tide gauge station data with the ensemble empirical mode decomposition method. *J Hydro Environ Res*. doi:[10.1016/j.jher.2014.12.002](https://doi.org/10.1016/j.jher.2014.12.002)
- Kim K-Y, North GR (1997) EOFs of harmonizable cyclostationary processes. *J Atmos Sci* 54:2416–2427
- Kim K-Y, North GR, Huang J (1996) EOFs of one-dimensional cyclostationary time series: computations, examples and stochastic modeling. *J Atmos Sci* 53:1007–1017
- Na H, Kim K-Y, Chang K-I, Kim K, Yun J-Y, Minobe S (2010) Interannual variability of the Korea strait bottom cold water and its relationship with the upper water temperatures and atmospheric forcing in the sea of Japan (East Sea). *J Geophys Res* 115:C09031. doi:[10.1029/2010JC006347](https://doi.org/10.1029/2010JC006347)
- Na H, Kim K-Y, Chang K-I, Park JJ, Kim K, Minobe S (2012) Decadal variability of the upper ocean heat content in the East/Japan sea and its possible relationship to northwestern Pacific variability. *J Geophys Res* 117:C02017. doi:[10.1029/2011JC007369](https://doi.org/10.1029/2011JC007369)
- Seo G-H, Cho Y-K, Choi B-J, Kim K-Y, Kim B-g, Tak Y-j (2014) Climate change projection in the Northwest Pacific marginal seas through dynamic downscaling. *J Geophys Res Oceans* 119:3497–3516. doi:[10.1002/2013JC009646](https://doi.org/10.1002/2013JC009646)
- Strassburg MW, Hamlington BD, Leben RR, Kim K-Y (2014) A comparative study of sea level reconstruction techniques using 20 years of satellite altimetry data. *J Geophys Res Oceans* 119:4068–4082. doi:[10.1002/2014JC009893](https://doi.org/10.1002/2014JC009893)
- Wu Z, Huang NE (2009) Ensemble empirical mode decomposition: a noise-assisted data analysis method. *Adv Adapt Data Anal* 1(1):1–41
- Yeo S-R, Kim K-Y (2014) Global warming, low-frequency variability, and biennial oscillation: an attempt to understand physical mechanism of the major ENSO events. *Clim Dyn* 43(3):771–786
- Youn YH, Oh IS, Park YH, Kim KH (2004) Climate variabilities of sea level around the Korean Peninsula. *Adv Atmos Sci* 21(4):617–626